energy&fuels

Article

pubs.acs.org/EF

Effect of Fuel Molecular Structure and Premixing on Soot Emissions from *n*-Heptane and 1-Heptene Flames

Xiao Fu, Xu Han, Kenneth Brezinsky, and Suresh Aggarwal*

Department of Mechanical & Industrial Engineering, University of Illinois at Chicago, 842 W. Taylor St., Chicago, Illinois 60607, United States

ABSTRACT: Most liquid fuels contain compounds with one or more unsaturated C=C bonds. Previous studies have observed that the fuel reactivity and ignition behavior are strongly influenced by the presence and number of double bonds in the fuel molecular structure. Here, we report a numerical investigation on the effect of fuel unsaturation on PAHs and soot emissions in partially premixed flames (PPFs) burning *n*-heptane and 1-heptene fuels. A detailed soot and fuel oxidation model is validated against gaseous species measurements in *n*-heptane PPF and soot measurements in ethylene diffusion flames. Simulations are performed to examine the effects of double bonds on PAHs and soot emissions at different strain rates and levels of premixing. For both fuels, the global flame structure is characterized by a rich premixed reaction zone (RPZ) on the fuel side and a nonpremixed reaction zone (NPZ) on the oxidizer side. PAHs and soot are mainly formed in the region between the RPZ and stagnation plane. The presence of double bonds results in higher amounts of C_2H_2 and PAHs, and thereby significantly higher soot emission in 1-heptene flames than that in *n*-heptane flames. As the level of premixing is reduced, spatial separation between the two reaction zones decreases, while C_2H_2 and PAH concentrations, and therefore soot emission, increase. The effect of fuel unsaturation on PAH and soot emissions becomes more pronounced as the level of premixing and/or the strain rate is reduced. A reaction path analysis was performed to identify the dominant routes for the formation of acetylene, benzene, and pyrene. Acetylene and benzene are known to be important precursors for larger PAH species, while acetylene also plays an important role in soot surface growth through the HACA mechanism. The analysis indicated that the major route for benzene formation in the RPZ is through the recombination reaction of propargyl radicals, which are mostly formed from allyl radicals. The other route is through the reaction of vinyl with butadiene. The presence of a double bond leads to higher concentrations of propargyl and butadiene and thus increased benzene formation in 1-heptene flames relative to that in *n*-heptane flames. The presence of a double bond also increases the amount of C_2H_2 formed in 1-heptene flames due to the higher C_4H_5 concentration. Thus, the presence of a double bond promotes β scission reactions, leading to the increased production of C_2H_2, C_6H_6, and $C_{16}H_{10}$ and thus higher soot emissions in 1-heptene flames.

1. INTRODUCTION

Modeling the oxidation chemistry of real fuels has been challenging, particularly for multidimensional simulations of reacting flows. Traditionally, simple surrogates have been considered to represent the combustion and emission behavior of these fuels. For instance, methane has been used to represent natural gas, while *n*-heptane and iso-octane have been considered as surrogates for diesel and gasoline fuels, respectively. However, there is increasing interest in considering more complex surrogates with varying compositions. This is driven by the need for developing reliable predictive tools for fuel-flexible combustion systems and the emergence of a new generation of renewable fuels. Since most conventional and emerging fuels contain compounds with one or more unsaturated C=C bonds, recent research has focused on the effect of these bonds on the fuel reactivity and ignition behavior. In this context, several experimental and modeling studies have examined the oxidation of straight chain C_5, C_6, and C_7 alkanes and alkene isomers. Ignition delay and speciation data have been reported from shock tube,[1−3] RCM,[4−6] and flow reactor[7] experiments. Detailed kinetic models have also been developed to provide further insight into the effects of the presence and position of double bonds on fuel reactivity and ignitibility. An important observation from these studies is that the fuel reactivity can vary significantly, especially in the NTC (negative temperature coefficient) region, depending upon the amount and type of isomers. The ignition delay time has been found to increase with the number of double bonds in the fuel molecular structure. With regard to the position of the double bond, the fuel ignitability has been observed to be strongly influenced by the length of the saturated portion aside the double bond, with the longer alkyl chain yielding a shorter ignition delay. While these studies have provided significant insight pertaining to fuel reactivity and ignitability, relatively little research has been reported concerning the combustion and emission behavior of unsaturated hydrocarbons. Motivated by this consideration, the present study examines the effect of the presence of a double bond on PAHs and soot emissions in flames. Partially premixed flames (PPFs) are simulated using two saturated and unsaturated fuels, namely *n*-heptane and 1-heptene, respectively.

Another motivation for the present study comes from recent engine experiments, which have observed that while PM (particulate matter) emissions are reduced using biodiesel fuels

Received: July 22, 2013
Revised: September 9, 2013
Published: September 10, 2013

   dx.doi.org/10.1021/ef401409r | *Energy Fuels* 2013, 27, 6262−6272

compared to conventional diesel, the amount of PM formed is strongly influenced by the presence and number of double bonds in the fuel molecular structure. Lapuerta et al.[8] reported diesel engine experiments with waste cooking oil and observed higher PM emissions with the increase in the number of double bonds or degree of unsaturation. Schönborn et al.[9] also observed higher PM emissions with the increase in the number of double bonds for fatty acid alkyl esters. Puhan et al.[10] performed single-cylinder experiments using linseed, jatropha, and coconut oils and reported increased emissions of CO, unburned hydrocarbons (UHCs), and smoke with the increase in the degree of unsaturation. Similarly, Benjumea et al.[11] conducted single-cylinder engine experiments with three different mixtures of fatty acid methyl esters and showed that smoke opacity and emissions of NO_x and UHC increased with the degree of unsaturation. In addition, a higher degree of unsaturation was found to increase the ignition delay and retard the start of combustion. Salamanca et al.[12] examined the effects of chemical composition of methyl esters on engine emissions and observed that linseed biodiesel produced more PM and UHC than palm biodiesel as a consequence of more unsaturated compounds in its composition, which favor the formation of soot precursors. To summarize, engine studies have generally found increased PM emissions due to the presence of unsaturation components in biodiesel fuels.

In order to explain these trends in engine emissions, there have been fundamental investigations on the formation of soot precursors during the combustion of unsaturated biodiesel components. Garner et al.[3] performed shock tube experiments using *n*-heptane (*n*-C_7H_{16}) and 1-heptene (1-C_7H_{14}) as analogs for the saturated and unsaturated hydrocarbon side chains of C_8 methyl esters and observed that 1-heptene produces more acetylene than does the *n*-heptane over intermediate temperatures, 1100−1600 K. Subsequently, Garner and Brezinsky[13] and Garner et al.[14] extended the study to the oxidation of methyl octanoate and methyl trans-2-octenoate and observed a longer ignition delay and increased acetylene (C_2H_2) formation in the case of unsaturated methyl ester. Note that acetylene provides a major route for soot particle surface growth through the "H-abstraction-C_2H_2-addition" (HACA) mechanism.[15,16] Sarathy at el.[17] compared two fatty acid methyl esters, methyl butanoate ($C_3H_7COOCH_3$) and its unsaturated counterpart methyl crotonate ($CH_3CH{=}CHCOOCH_3$), in a counterflow diffusion flame and jet stirred reactor. Methyl crotonate was observed to produce a higher amount of acetylene, propyne (1-C_3H_4), 1-butene (1-C_4H_8), 1,3-butadiene (1,3-C_4H_6), and benzene (C_6H_6), indicating the potential of increased soot formation with unsaturated biodiesel fuels compared to the saturated ones. Our previous studies[18,19] on *n*-heptane and 1-heptene partially premixed counterflow flames (PPFs) revealed that unsaturated fuel, 1- heptene, produces higher amounts of acetylene and benzene compared to saturated fuel, *n*-heptane. Further analysis indicated that the dominant path for benzene formation involves the recombination of propargyl radicals (C_3H_3), and the presence of the double bond in 1-heptene provides a significant route for its production through the formation of an allyl radical (C_3H_5). This path is not favored in the oxidation of *n*-heptane, as it decomposes directly to smaller alkyl radicals.

The present work extends our previous investigation and examines the effect of the presence of a double bond on PAHs and soot formation in PPFs burning prevaporized *n*-heptane and 1-heptene fuels. Since these fuels represent the hydrocarbon side chains of the saturated and unsaturated methyl esters, namely methyl octanoate and methyl *trans*-2-octenoate, the study is also relevant to the understanding of soot emissions from the combustion of biodiesel fuels. Since these fuels represent the hydrocarbon side chains of the saturated and unsaturated methyl esters, namely methyl octanoate and methyl *trans*-2-octenoate, the study is also relevant to the understanding of soot emissions from the combustion of biodiesel fuels. Moreover, *n*-heptane has often been used as a surrogate for diesel fuel. Another objective is to characterize the soot formation processes in a flame environment containing regions of both rich premixed and nonpremixed combustion, for which relatively little research has been reported. The PPFs have been simulated in an opposed jet flow configuration because of its simple flow field and its relevance to diesel engine combustion.[20] The soot processes considered include nucleation, surface growth and oxidation, and coagulation. The coagulation process is modeled using Frenklach's method of moments approach. The soot model is combined with a detailed fuel oxidation and NO_x formation model involving 198 species and 4932 reactions. The combined model is validated using hydrocarbon species and benzene measurements in *n*-heptane PPFs[21] and soot measurements in ethylene diffusion flames.[22] Simulations are performed to characterize the effects of double bonds, the level of partial premixing (or equivalence ratio), and strain rates on the PAHs and soot emissions.

2. THE PHYSICAL-NUMERICAL MODEL

The counterflow flame configuration employed in the present investigation is shown schematically in Figure 1. It consists of two

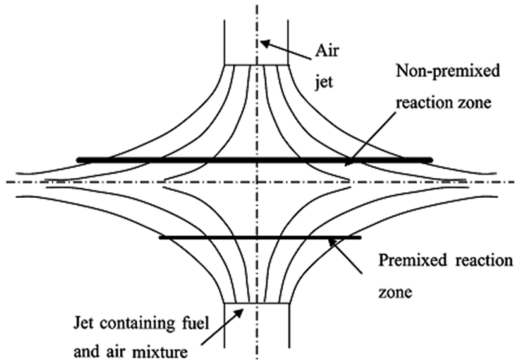

Figure 1. A schematic of the opposed jet configuration for partially premixed flames.

opposing jets issuing from two coaxial nozzles that are placed one above the other. A partially premixed configuration containing two reaction zones is established by having a fuel rich stream with a specified equivalence ratio (ϕ) from the lower nozzle and an air stream from the upper nozzle. Depending upon the value of ϕ, a significant amount of soot formation is expected in the region between the rich premixed zone and the stagnation plane. The separation distance between the nozzles is 1.5 cm in this study. Since the fuel is considered in the vaporized form, the fuel stream temperature is assumed to be 400 K and the oxidizer stream temperature as 300 K. N-heptane and 1-heptene PPFs are established by independently varying ϕ and the global strain rate (a_G),[23] which is expressed as

$$a_G = \frac{2\nu_o}{L}\left(1 + \frac{\nu_f\sqrt{\rho_f}}{\nu_o\sqrt{\rho_o}}\right) \quad (1)$$

Here, L denotes the separation distance between the two nozzles; ν_f, the fuel jet inlet velocity; ν_o, the oxidizer jet inlet velocity; and ρ_f and

dx.doi.org/10.1021/ef401409r | Energy Fuels 2013, 27, 6262−6272

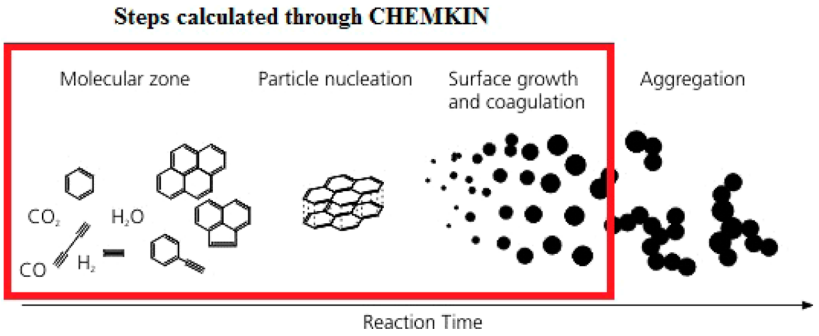

Figure 2. Soot formation process. Red box indicates the formation processes considered in the current model.

ρ_o, the mixture densities in the fuel and oxidizer streams, respectively. The inlet velocities of the fuel and oxidizer streams were specified by matching the momentum of the two streams for given ϕ and a_G. For this investigation, the strain rate was varied from 50 s^{-1} to 350 s^{-1}. At higher strain rates, a_G > 350 s^{-1}, the amount of soot formed was very small due to the small resident time.

Simulations are performed using the OPPDIF in CHEMKIN Pro 15113 package.[24] The reaction mechanism used to model *n*-heptane and 1-heptene flames has been developed previously by extending a detailed oxidation scheme[25,26] for several fuels. Due to the hierarchical modularity of the mechanistic scheme, the model is based on a detailed submechanism of C_1-C_4 species. Investigation on the formation of the first aromatic rings by C_2 and C_4 chemistry and by resonance-stabilized radicals, such as propargyl (C_3H_3) and allyl (C_5H_5), has been performed by Goldaniga et al.[26] The NO_x mechanism is adopted from various sources. It includes the thermal NO,[27] prompt NO,[28] intermediate N_2O,[29] and intermediate NNH[30] submechanisms. Details on these submechanisms have been provided in a previous investigation.[18] Results concerning the effect of fuel unsaturation on NO_x emissions have been reported in the cited study and are not repeated here.

Figure 2 presents a schematic of the soot formation processes.[31] As fuel decomposition is initiated, intermediate hydrocarbon species are formed in the fuel rich regions, which undergo further reactions to form PAHs. Once a primary particle is formed through nucleation and polymerization, it can grow through surface reactions and coagulation and also undergo oxidation. The kinetic model used for fuel oxidation is capable of simulating the formation of PAHs up to pyrene ($C_{16}H_{10}$). Particle inception is modeled by a nucleation reaction with two pyrene molecules as the reactants. The nucleation reaction is an irreversible reaction, which provides the particle inception rate and defines the size and the surface coverage of the particle (or nucleus). The nuclei start to interact with each other through coagulation as well as with the gaseous species on its surface. The dynamics of coagulation can be modeled by solving particle size distribution functions (PSDFs) using either a discrete-sectional method[32] or the method of moments.[33] Although more accurate, discrete methods are known to be computationally very expensive and are not considered here. Instead, the method of moment approach, developed by Frenklach et al.,[33,34] is used to describe the moments of the PSDFs. The approach provides the average properties of soot population without a priori knowledge of PSDF and therefore requires significantly fewer computational resources. The soot formation model also includes surface reactions with gaseous species to determine the surface growth and oxidation rates. The soot aggregation is not considered in the present study. Numerical simulations are performed to examine the effects of fuel molecular structure, equivalence ratio, and strain rate on PAHs and soot emissions in PPFs.

3. RESULTS AND DISCUSSION

3.1. Model Validation. As discussed by Frenklach, the simulation of flame sooting characteristics involves two major components, namely the gas-phase chemistry and soot particle dynamics. Thus, the accuracy of the particle dynamics model relies on an accurate prediction of the gaseous species, which determines the particle nucleation and surface growth rates.

While the present kinetic model has been extensively validated in previous studies, we provide herein an additional validation using the measurements of Berta et al.[21,35] for an *n*-heptane PPF established at ϕ = 4.27, a_G = 100 s^{-1}, and a nitrogen dilution of 17%. In an earlier investigation,[35] the validation has been performed for four different PPFs with ϕ = 2.5, 4.27, 12.6, and 15.3. The comparison indicated that for these four cases, the difference in predicted and measured peak temperatures ranged between 2 and 7%, while that in peak benzene mole fractions ranged between 20% and 30%. For the ϕ = 4.27 case, Figure 3 presents the predicted and measured

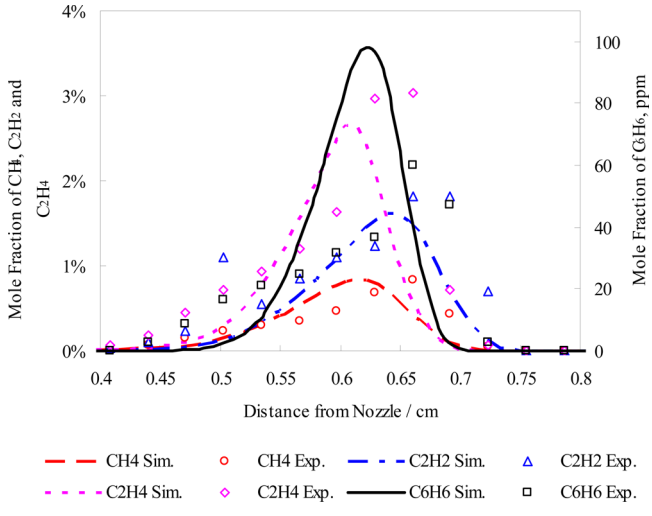

Figure 3. Predicted (lines) and measured[21] (symbols) flame structures in terms of species mole fraction profiles for *n*-heptane partially premixed flame at ϕ = 4.27, a_G = 100 s^{-1}, and nitrogen dilution of 17%, which contains CH_4 (○), C_2H_2 (△), C_2H_4 (◊), and C_6H_6 (□) profiles.

mole fraction profiles for several hydrocarbon species including benzene. There is generally good agreement between predictions and measurements, especially with respect to intermediate hydrocarbon (C_2H_2, C_2H_4, and CH_4) species profiles. However, the model overpredicts the peak benzene mole fraction by about 25% compared to measurements.

A validation of the soot model is shown in Figure 4, which presents a comparison of the predicted soot volume fraction profiles with the measurements of Hwang and Chung[36] and Vansburger et al.[37] in a counterflow ethylene diffusion flame. For these results, the separation distance between the fuel and oxidizer nozzles was 1.42 cm, and the exit velocities of both fuel

dx.doi.org/10.1021/ef401409r | Energy Fuels 2013, 27, 6262−6272

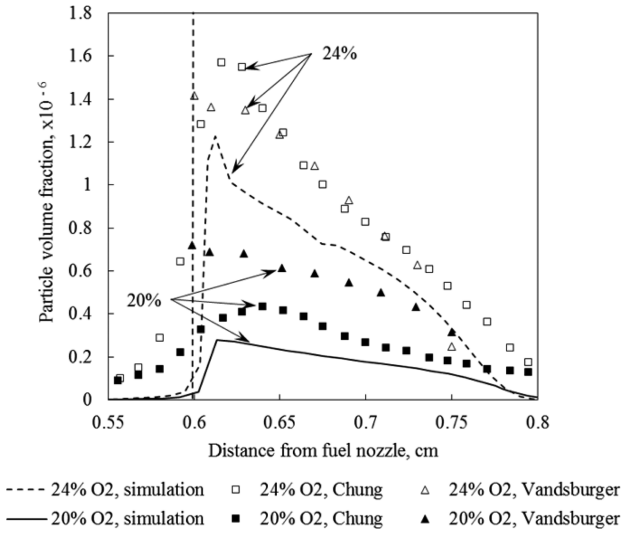

Figure 4. Predicted (lines) and measured (symbols) soot volume fraction profiles for pure C_2H_4 diffusion flame. Fuel and oxidizer nozzle exit velocities are both 19.5 cm/s. Nozzle separation length is 1.42 cm. (△) Experimental data from Vansburger et al.[37] (□) Experimental data from Hwang and Chung.[36] The mole fraction of O_2 in the oxidizer stream is 24% and 20% for the two cases. Vertical line represents the stagnation plane.

and oxidizer streams were 19.5 cm/s. Results are shown for two compositions of the oxidizer stream, namely 20% O_2 + 80% N_2 and 24% O_2 + 76% N_2 by volume. The fuel stream contained pure C_2H_4. There is generally good agreement between the predictions and measurements for both the cases, with the numerical model underpredicting soot volume fractions by about 20% to 30%. In addition, the soot inception seems to occur earlier, and the soot volume fraction profiles are wider in the experimental study. This may be attributed to the fact that soot aggregation is not included in our soot model. Soot aggregation is expected to increase the soot particle size, and the diffusion of larger particles may affect the predicted soot volume fraction profiles. However, similar discrepancies between predictions and measurements have been reported by Liu et al.,[38] who attributed them to the lack of information on experimental conditions including boundary conditions. Consequently, they adjusted the separation distance between the two nozzles and the surface growth rate in their model in order to achieve better agreement with the measurements of Hwang and Chung. Moreover, as Figure 4 indicates, there are also differences between the two sets of measurements apparently for the same conditions. In view of these factors, the prediction of soot emission using the present model is deemed acceptable.

3.2. Structure of *n*-Heptane and 1-Heptene Partially Premixed Flames. In order to gain insight into the effect of an unsaturated bond on soot formation and oxidation processes, we present in Figure 5 the structures of *n*-heptane and 1-heptene partially premixed flames (PPFs) computed at $\phi = 2$ and $a_G = 50\ s^{-1}$. Several gaseous and soot properties are plotted versus distance from the fuel nozzle. The gaseous properties include profiles of temperature, axial velocity, heat release rate (HRR), and mole fractions of oxygen, acetylene, and pyrene. The soot properties include the average particle diameter, particle number density, and soot volume fraction. The global flame structures for the two fuels are generally similar, implying that the overall combustion process is not strongly influenced by the presence of the unsaturated bond.

For both fuels, the HRR profile contains two peaks, one corresponding to the rich premixed reaction zone (RPZ) located on the fuel side and the other indicating the nonpremixed reaction zone (NPZ) located close to the stagnation plane. Note that the locations of the stagnation plane, RPZ and NPZ, are indicated by vertical lines in Figures 5 and 6. As discussed in a previous study,[35] the fuel is completely pyrolyzed/oxidized to produce CO, H_2, and hydrocarbon species in RPZ, while the NPZ is characterized by the oxidation of CO and H_2. Species profiles in Figure 5 indicate that acetylene is mainly formed in the RPZ, while pyrene (PAHs) is formed both in the RPZ and region between RPZ and stagnation plane. In contrast, the peak temperature occurs in the NPZ, where most of H_2O and CO_2 are produced. The particle number density profiles indicate that nucleation is initiated with the formation of PAH species, pyrene. Subsequently, the particle diameter and soot volume fraction continue to increase due to surface reactions and coagulation in the region between the RPZ and stagnation plane. The number density, which is determined by a competition between nucleation and coagulation, also increases in this region. The peaks in particle diameter and soot volume fraction are located between RPZ and NPZ due to a long residence time in this region. Moreover, there is noticeable soot oxidation in the region between the two reaction zones, due to the diffusive transport of O_2 into this region, as indicated by O_2 profiles. Both the number density and soot volume fraction become zero right after crossing the stagnation plane. However, the average particle diameter becomes zero at some finite distance from the stagnation plane, suggesting that only a very small amount of soot diffuses to the oxidizer side where it gets oxidized.

3.3. Effect of Partial Premixing on Soot Formation in PPFs. Figure 6 presents the computed structures of *n*-heptane and 1-heptene partially premixed flames (PPFs) under the same conditions as those for Figure 5, except that $\phi = 8$. Similar to the case for $\phi = 2$ (cf. Figure 5), the global flame structures for the two fuels are again similar, implying that the overall fuel oxidation and heat release processes are not strongly influenced by the presence of the unsaturated bond. However, the flame structure and soot formation are markedly influenced by the level of partial premixing, i.e., as ϕ is increased from 2 to 8. For the latter case, the RPZ is located very close to the stagnation plane, while the NPZ is located on the oxidizer side. The RPZ is also considerably weaker compared to the NPZ, where most of the heat release occurs. However, the concentrations of hydrocarbon species, especially PAHs, in the RPZ are significantly higher as ϕ is increased from 2 to 8. For instance, the peak pyrene mole fraction in the *n*-heptane flame increases from 1.7×10^{-9} to 1.9×10^{-6} as ϕ is increased from 2 to 8, and this can be attributed to two factors. One is the effect of ϕ, which increases the concentration of hydrocarbon species due to their reduced oxidation rate. The other factor is the increased residence time since RPZ is now located near the stagnation plane. Thus, the peaks in acetylene and pyrene profiles are located close to the stagnation plane. Consequently, the peaks in particle number density and soot volume fraction profiles are also located near the stagnation plane, and their values are considerably higher compared to those for $\phi = 2$. The O_2 profiles indicate relatively little soot oxidation for this case compared to that for $\phi = 2$, since the soot particles formed

dx.doi.org/10.1021/ef401409r | Energy Fuels 2013, 27, 6262−6272

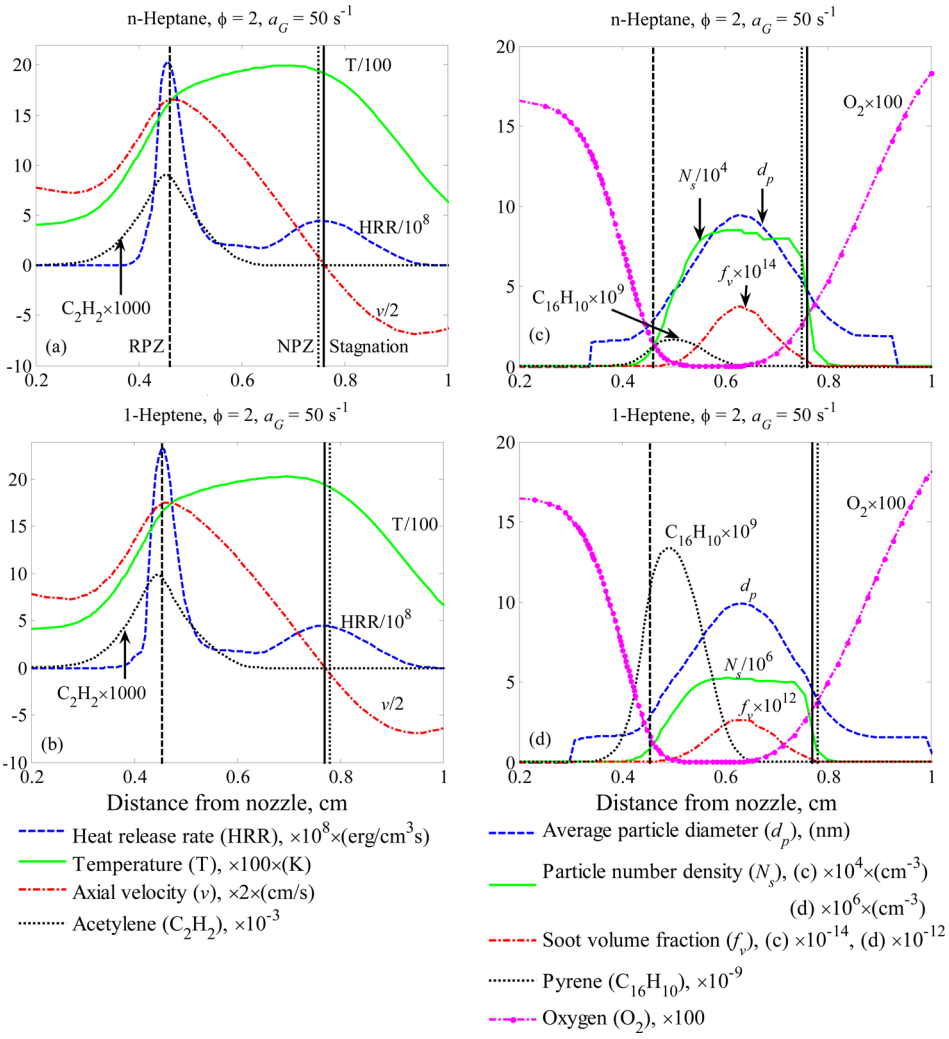

Figure 5. Flame structures of *n*-heptane and 1-heptene PPFs at ϕ = 2, a_G = 50 s^{-1}. (a and b) Temperature, heat release rate, axial velocity, and acetylene mole fraction. (c and d) Average particle diameter (d_p), particle number density (N_s), soot volume fraction (f_v), pyrene mole fraction, and oxygen mole fraction. Vertical lines represent locations of the stagnation plane, rich premixed zone (RPZ), and nonpremixed zone (NPZ), as noted in part a.

near NPZ are pushed away from this zone toward the stagnation plane. Moreover, there is little oxygen in this region. Thus, for the PPFs investigated in this study, the soot emission is predominantly due to nucleation and surface growth, with the latter caused by surface reactions and coagulation, while the amount of soot oxidation depends upon the level of partial premixing. Another important observation from Figures 5 and 6 is that while the amount of soot produced is still noticeably higher in 1-heptene flame compared to that in *n*-heptane flame at all equivalence ratios, the effect of the double bond becomes less pronounced at higher ϕ.

3.4. Effect of Fuel Molecular Structure on PAH and Soot Emissions. As discussed in previous studies,[17,19] unsaturated fuels produce higher amounts of hydrocarbons, especially C_2H_2, C_3H_3, and C_6H_6, resulting in increased PAH emissions. This is supported by the simulation results presented in Figures 5 and 6, which indicate a significantly higher pyrene concentration in the 1-heptene flame compared to that in the *n*-heptane flame. As a consequence, the soot number density and volume fraction are also noticeably higher in 1-heptene flames compared to those in *n*-heptane flames. These differences can be attributed to the increased amounts of C_2H_2, C_3H_3, C_6H_6, and $C_{16}H_{10}$ and are related to the presence of a double bond in 1-heptene. This is illustrated more clearly in Figures 7 and 8, which plot the peak values of PAHs and soot properties for different flame conditions for the two fuels. As indicated in Figure 7, at any given ϕ and a_G, the peak mole fractions of C_2H_2, C_6H_6, and pyrene are noticeably higher in 1-heptene flames compared to those in *n*-heptane flames. Consequently, as indicated in Figure 8, the particle diameter, number density, and soot volume fraction are significantly higher in 1-heptene flames compared to those in *n*-heptane flames. Moreover, the effect of the double bond is more pronounced at lower ϕ and higher a_G, except that the difference in particle diameter between two fuels is higher in ϕ = 8 flames compared to ϕ = 2 flames. Thus, as the level of partial premixing is increased, or as the strain rate is increased, the effect of the double bond on PAHs and soot emissions becomes more pronounced. Note, however, that the PAHs and soot emissions are noticeably reduced as the strain rate and/or the level of partial premixing is increased.

The increased soot emission as a consequence of double bonds in the fuel molecular structure is related to the higher nucleation and surface growth rates, which are due to the

dx.doi.org/10.1021/ef401409r | *Energy Fuels* 2013, 27, 6262−6272

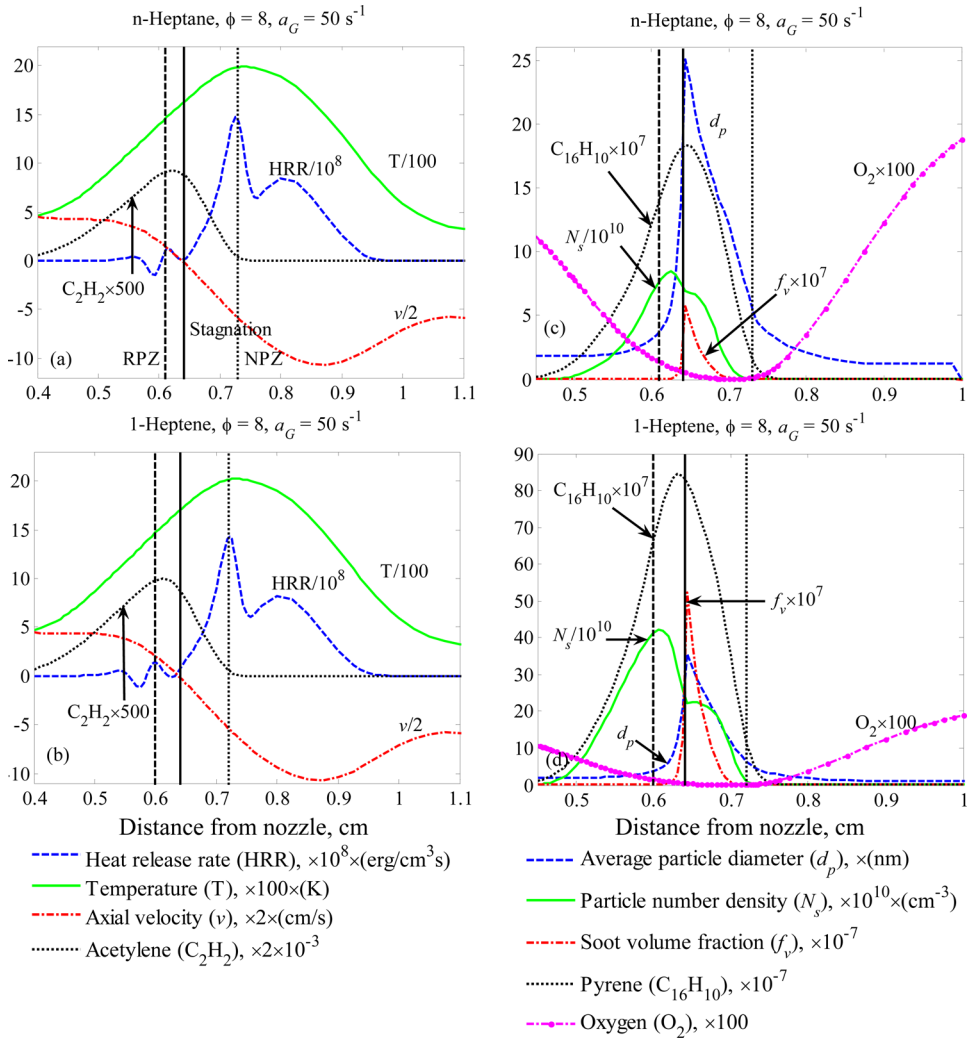

Figure 6. Flame structures of *n*-heptane and 1-heptene PPFs at ϕ = 8 and a_G = 50 s^{-1}. (a and b) Temperature, heat release rate, axial velocity, and acetylene mole fraction. (c and d) Average particle diameter (d_p), particle number density (N_s), soot volume fraction (f_v), pyrene mole fraction, and oxygen mole fraction. Vertical lines represent locations of the stagnation plane, rich premixed zone (RPZ), and nonpremixed zone (NPZ), as noted in part a.

increased production of $C_{16}H_{10}$ and C_2H_2 in 1-heptene flames compared to that in *n*-heptane flames. The nucleation process in the present soot model is represented by

$$2C_{16}H_{10} \Rightarrow 32C + 20C_{soot}{-}H + 28.75C_{soot}^{\bullet} \quad (2)$$

In this reaction, two pyrene molecules combine to form one soot nucleus containing 32 C atoms. The $C_{soot}{-}H$ is a carbon atom site with surface-bonded hydrogen atom, while the $C_{soot}^{\bullet}$ is an open (or empty) surface site. The surface site density is defined as the number of active chemical sites per surface area where adsorption, desorption, and chemical reaction can take place. Here, 20 of the C atoms have H surface sites, and about 28.75 of the 32 C atoms are open sites. The $C_{soot}{-}H$ and $C_{soot}^{\bullet}$ sites then react with gaseous species through surface growth reactions 3−6, as described by the HACA (hydrogen abstraction, acetylene addition) mechanism.

The particle number density is determined by competition between the nucleation and coagulation processes, while the soot particle diameter and volume fraction are determined by the coagulation and surface reaction rates. As discussed by Frenklach and Harris,[34] the coagulation of soot particles is based on Smoluchowski's theory of Brownian motion[32] and proportional to the square of the total particle number, while the surface growth is modeled through the HACA mechanism, represented by reactions

$$H + C_{soot}{-}H \Leftrightarrow C_{soot}^{\bullet} + H_2 \quad (3)$$

$$C_{soot}{-}H + OH \Leftrightarrow H_2O + C_{soot}^{\bullet} \quad (4)$$

$$C_{soot}^{\bullet} + H \Rightarrow C_{soot}{-}H \quad (5)$$

$$C_{soot}^{\bullet} + C_2H_2 \Rightarrow C_{soot}{-}H + 2C + H \quad (6)$$

As indicated, C_2H_2, H, and OH are the gaseous species involved in this mechanism. In reaction 6, a C_2H_2 molecule attaches to the $C_{soot}^{\bullet}$ site and forms $C_{soot}{-}H$ and H. In addition, two carbons are added to the carbon bulk. Finally, the soot oxidation is determined by the following reaction:

$$OH + C_{soot}^{\bullet} + C \Leftrightarrow C_{soot}{-}H + CO \quad (7)$$

Results pertaining to the effects of equivalence ratio, strain rate, and fuel unsaturation on soot emission in *n*-heptane and 1-heptene flames can be explained by the soot particle dynamics model discussed above. First of all, the particle number density, which is determined by a competition between nucleation and

dx.doi.org/10.1021/ef401409r | Energy Fuels 2013, 27, 6262−6272

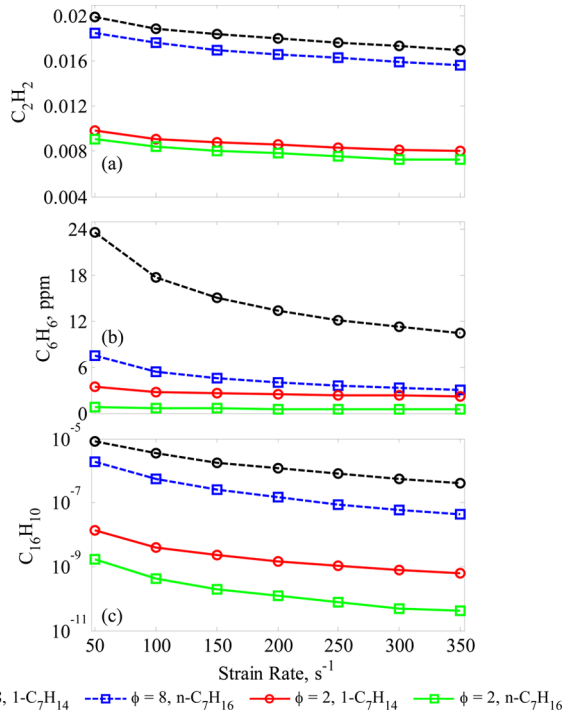

Figure 7. Peak mole fractions of acetylene (C_2H_2), benzene (C_6H_6), and pyrene ($C_{16}H_{10}$) plotted versus strain rate for *n*-heptane and 1-heptene PPFs at ϕ = 2 and 8. Note that pyrene is plotted on a log scale.

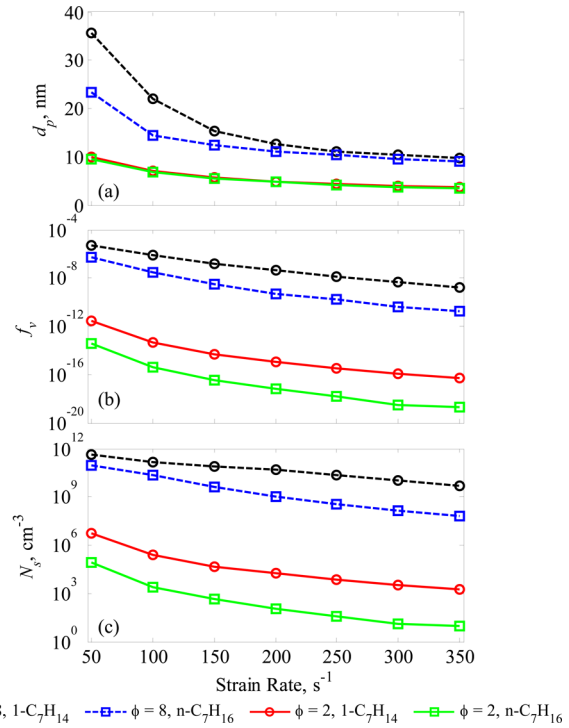

Figure 8. Peak soot diameter (a), number density (b), and volume fraction (c) plotted versus strain rate for *n*-heptane and 1-heptene PPFs at ϕ = 2 and 8. Note that the number density and volume fraction are plotted on a log scale, and soot diameter is plotted on a linear scale.

coagulation, is considerably higher in 1-heptene flames than in *n*-heptane flames. This can be attributed to the significantly higher nucleation rate due to the increased pyrene production in 1-heptene flames. Note that the pyrene concentration also increases as ϕ is increased and/or the strain rate is decreased. Consequently, the soot emission increases with the increase in ϕ and/or decrease in a_G. Second, the particle diameter is higher in 1-heptene flames since the coagulation and surface reaction rates are higher in these flames. The coagulation rate is higher due to the higher particle population, while the surface reaction rates are higher due to the increased C_2H_2 production in 1-heptene flames than in *n*-heptane flames, as noted earlier in the context of Figures 5 and 6. Consequently, the soot volume fraction is also higher in 1-heptene flames due to the higher nucleation and surface reaction rates. However, for ϕ = 2 flames, the difference in particle diameter between two fuels is less noticeable compared to ϕ = 8 flames, which is mainly due to low C_2H_2 concentration near the location of peak of particle diameter in ϕ = 2 flames. Finally, as noted earlier, for the PPFs simulated in this study, the soot oxidation is negligible in ϕ = 8 flames but becomes important in ϕ = 2 flames.

The effect of strain rate on soot emissions is illustrated in Figure 9, which presents the profiles number density and soot particle diameter in *n*-heptane PPFs at a_G = 50 s^{-1} and 350 s^{-1} and ϕ = 2. The HHR profiles are also included to indicate the RPZ and NPZ locations. As expected, the HHR increases at higher strain rates due the higher fuel flow rate. In addition, with the increase in strain rate, the separation between the RPZ and NPZ decreases, since the RPZ moves farther away from fuel nozzle, and is established at a location where the strained premixed flame speed matches the local flow velocity. The NPZ location, which is close to the stagnation plane, is not much affected by the change in strain rate. More importantly, as the strain rate is increased, the soot number density and particle diameter decrease noticeably due to the reduced residence time at higher strain rates. The soot volume fraction exhibits similar behavior with respect to the strain rate and is therefore not shown. Similarly, the soot property profiles for 1-heptene flames are not shown, as these profiles were qualitatively similar to those for *n*-heptane flames, although there was significantly higher soot production in 1-heptene flames, as discussed earlier. In summary, while the presence of a double bond causes a significant increase in soot emissions in PPFs, the effect is more noticeable at low strain rates. For instance, for the conditions investigated, there is little soot formation at strain rates higher than 350 s^{-1}.

3.5. Reaction Path Analysis for PAH Formation in PPFs. As discussed in the preceding sections, there is significantly higher PAH and soot production in 1-heptene flames than in *n*-heptane flames. Since C_2H_2 and C_6H_6 are the major precursors for soot, an analysis was performed to identify the dominant pathways for their formation in these flames. The analysis considered a region between the RPZ and stagnation plane, where most of the PAHs and soot are formed. Results are presented in Figure 10, which summarizes the major pathways for C_2H_2 and C_6H_6 formation in *n*-heptane and 1-heptene flames at ϕ=2.0 and strain rate of 50 s^{-1}. While the oxidation of the two fuels follows different paths, benzene is mainly formed through the recombination reaction of propargyl (C_3H_3) radicals.[39] Most of C_3H_3 is formed from allyl radical (C_3H_5), and its formation from fuel decomposition is quite different for the two fuels, as can be seen in Figure 10. At high temperatures (>1200K), typical of flame environment, most of 1-heptene directly decomposes into C_3H_5 and C_4H_9, as a consequence of the β scission reaction due to the presence of

dx.doi.org/10.1021/ef401409r | *Energy Fuels* 2013, 27, 6262−6272

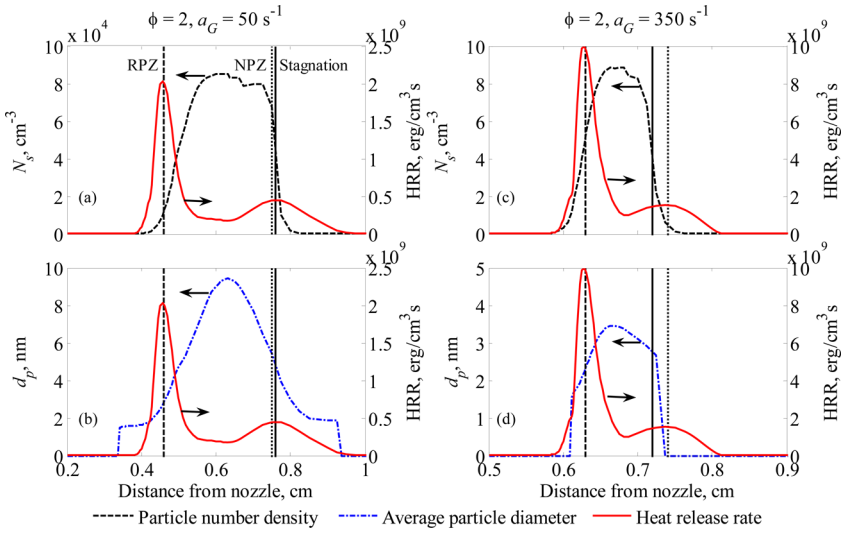

Figure 9. Effect of strain rate on soot emission in *n*-heptane PPF. Profiles of particle number density, N_s (a and c), and particle diameter, d_p (b and d), for PPFs at $\phi = 2$ and strain rates of 50 s^{-1} (a and b) and 350 s^{-1} (c and d). Heat release rate (HRR) profiles are also shown (solid line). Vertical lines represent locations of the stagnation plane, rich premixed (RPZ), and nonpremixed reaction zones (NPZ), as noted in part a.

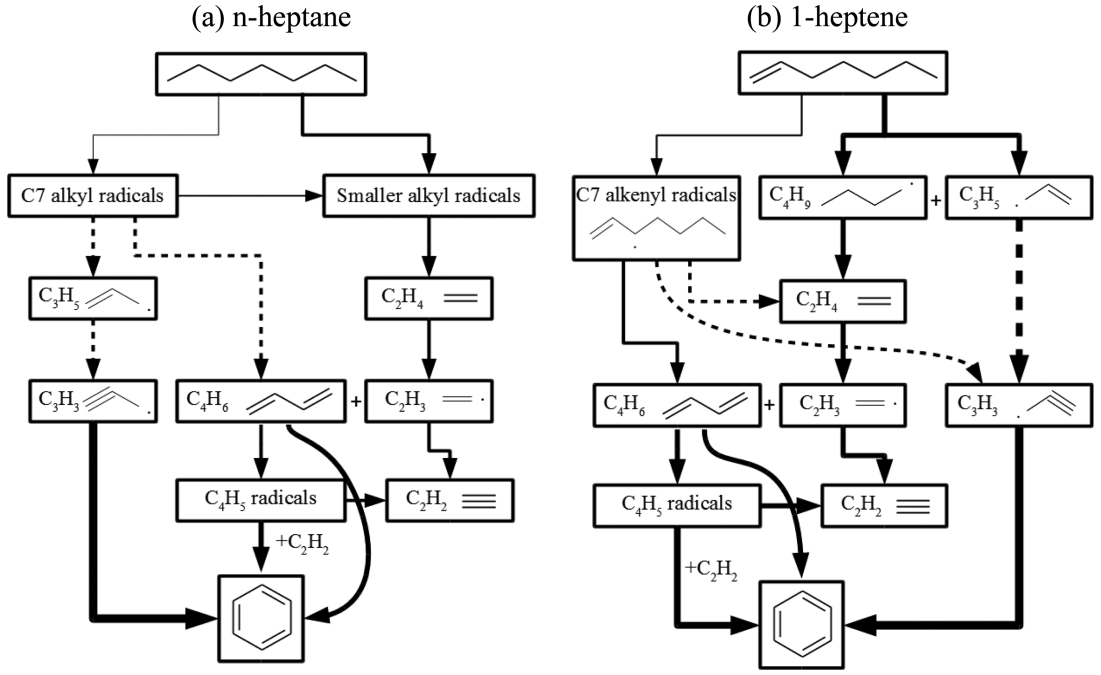

Figure 10. Dominant acetylene and benzene formation paths in *n*-heptene (a) and 1-heptene (b) established at $\phi = 2.0$ and a strain rate of 50 s^{-1}. Arrows with dashed lines indicate multiple reactions, while the arrow thickness indicates the relative contribution of each reaction or path.

double bond in 1-heptene. [Note the presence of double bond strengthens the adjacent C−C or C−H bond (α bond), while making the next C−C bond or C−H bond (β bond) weaker. The scission of C−C bond at the β position is defined as β scission.] In contrast, the decomposition of *n*-heptane mostly leads to the formation of various alkyl radicals, such as CH_3, C_6H_{13}, C_2H_5, C_5H_{11}, C_3H_7, and C_4H_9, via the C−C bonds scission, most of which then decompose to produce C_2H_4 and CH_3 (not shown) through β scission and H abstraction reactions. In addition, the butyl (C_4H_9) formed from 1-heptene also decomposes to produce C_2H_4, which is the main path for the formation of ethylene in the 1-heptene flame (cf. Figure 10b), while there are multiple alkyl species (C_6H_{13}, C_5H_{11}, C_4H_9, C_3H_7, etc.) that form ethylene in the *n*-heptane flame (cf. Figure 10a). Consequently, the ethylene concentration is higher in *n*-heptane flames compared to that in 1-heptene flames, as indicated in Figure 11a. Ethylene subsequently forms vinyl (C_2H_3), which produces additional benzene through its reaction with 1,3-butadiene (C_4H_6). Note, however, that higher C_2H_4 concentration does not imply increased benzene production in *n*-heptane flames, since the butadiene concentration is much lower in this flame compared to that in 1-heptene flames (cf. Figure 11b). The latter is due to the fact that the formation of allyl competes with that of butadiene in *n*-heptane flames, unlike the case for 1-heptene flames, in which the path to butadiene is preferred. The above pathway from fuel to benzene formation as well as the observations regarding the importance of allylic radicals, propargyl, vinyl, and butadiene

dx.doi.org/10.1021/ef401409r | *Energy Fuels* 2013, 27, 6262−6272

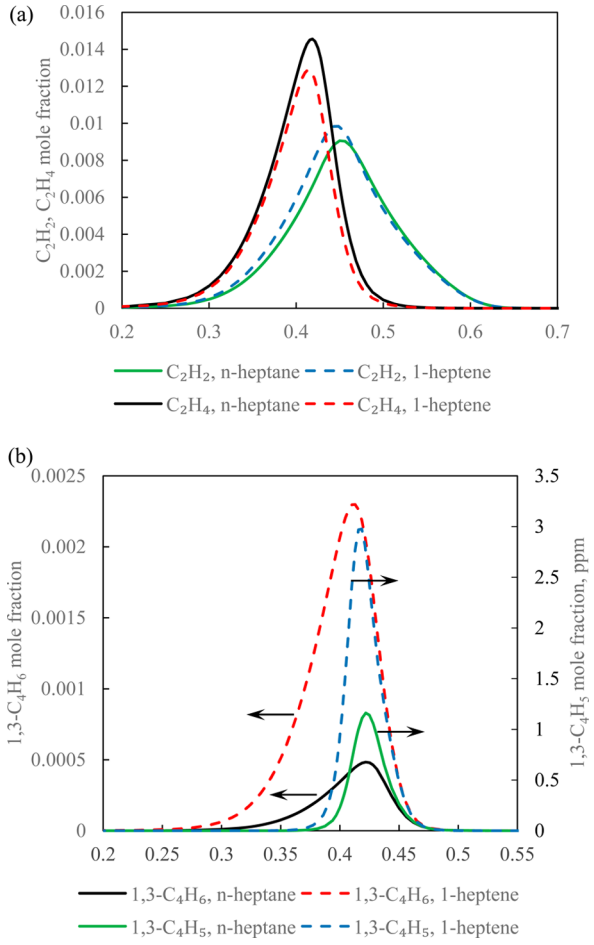

Figure 11. Comparison of C_2H_2 and C_2H_4 profiles (a) and 1,3-C_4H_6 and 1,3-C_4H_5 profiles (b) in *n*-heptane (solid lines) and 1-heptene (dashed lines) partially premixed flames at $\phi = 2$, $a_G = 50\ s^{-1}$.

are consistent with previous studies; see, for example, Zhang et al.,[40,41] who examined the chemistry of aromatic precursor formation in *n*-heptane premixed flames, and Han et al.,[19] who analyzed the effect of fuel unsaturation on the formation of C_2H_2 and C_6H_6 in triple flames.

Furthermore, it is important to mention that the presence of double bonds also leads to the increased production of C_2H_2 in 1-heptene flames than in *n*-heptane flames. As indicated in Figure 10, C_2H_2 is mainly formed from vinyl and produces benzene through its reaction with the C_4H_5 radical, which is formed from butadiene. While the concentration of C_2H_4 is higher in *n*-heptane flames, as noted above, that of C_2H_2 is higher in 1-heptene flames. This is due to the fact that C_2H_2 is produced from both C_2H_4 (through vinyl) and C_4H_5 (which breaks down to form C_2H_2 and C_2H_3), and the C_4H_5 concentration is noticeably higher in 1-heptene flames (cf. Figure 11b), leading to the increased production of C_2H_2 in these flames. Acetylene subsequently plays an important role in the formation of larger PAH species through the HACA (hydrogen abstraction acetylene addition) mechanism. In summary, the presence of a double bond in unsaturated hydrocarbon (1-heptene) promotes β scission reactions leading to the increased production of C_2H_2 and C_6H_6 and thereby higher pyrene and soot emissions.

A pathway analysis was also performed for the formation of pyrene, which is considered as the major nucleating species for soot formation. As indicated in Figure 12, for both the fuels, benzene is a major precursor for pyrene ($C_{16}H_{10}$) formation. Once the first aromatic ring is formed, it undergoes multiple routes, preferably through the phenyl (C_6H_5) radical and styrene (C_8H_8) to form phenylacetylene (C_8H_6). Then two phenylacetylene molecules can form pyrene and H_2. Another major pyrene formation path is from shorter chain alkene and alkenyl, such as C_5, C_4, and C_2, species. These can form a cyclopentadienyl radical (C_5H_5). Then two cyclopentadienyls can produce H_2 and naphthalene ($C_{10}H_8$), while the latter can subsequently form acenaphthylene ($C_{12}H_8$) through HACA

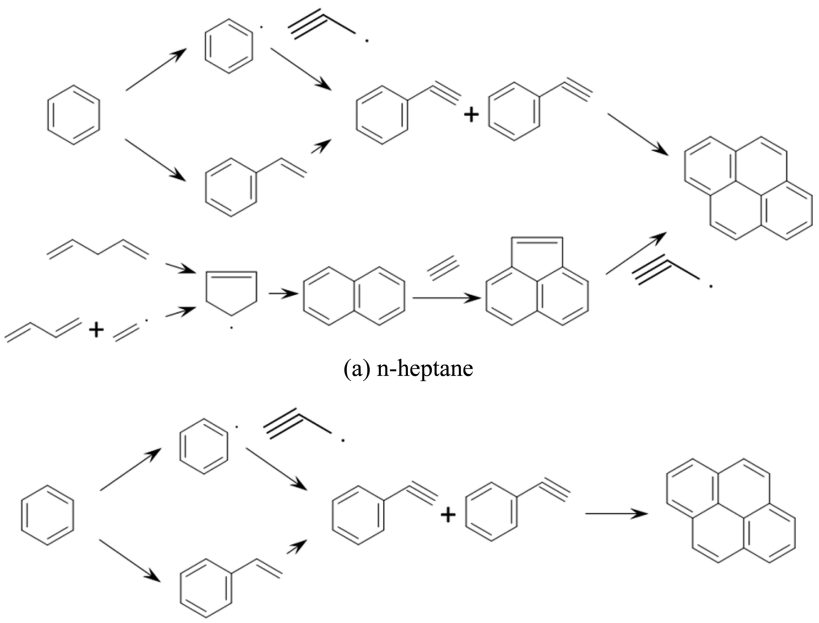

Figure 12. Dominant pyrene formation path in *n*-heptane (a) and 1-heptene (b) flames.

dx.doi.org/10.1021/ef401409r | *Energy Fuels* 2013, 27, 6262−6272

reactions. Finally, one acenaphthylene reacts with one propargyl (C_3H_3) to form half the pyrene and half the phenanthrene ($C_{14}H_{10}$). However, the pyrene formation through the cyclopentadienyl route is significantly less important compared to the benzene route. Other pyrene formation paths under the flame conditions are even less important than the cyclopentadienyl route and are not shown. As noted earlier, benzene is more pronounced in 1-heptene flames, making the benzene route the most significant pyrene formation path in 1-heptene flames. Thus, the increased formation of pyrene can be related to the higher concentrations of C_2H_2 and C_6H_6.

4. CONCLUSIONS

A numerical investigation was conducted to examine the effect of fuel unsaturation on PAH and soot emissions in partially premixed flames (PPF) burning *n*-heptane and 1-heptene fuels. A detailed soot model was combined with a fuel oxidation and NO_x chemistry model containing 198 species and 4932 reactions. Soot processes considered in the model include nucleation, surface growth, oxidation, and coagulation, based on the Frenklach method of moments approach. The combined model was validated using gaseous species measurements in *n*-heptane PPFs and soot measurements in ethylene diffusion flames. Simulations were performed to characterize the effects of double bonds, the level of premixing, and strain rates on PAHs and soot emissions. Important conclusions follow.

For both fuels, the global flame structure is characterized by a rich premixed reaction zone (RPZ) on the fuel side and a nonpremixed reaction zone (NPZ) located close to the stagnation plane or on the oxidizer side. The fuel is completely pyrolyzed/oxidized to produce CO, H_2, and hydrocarbon species (including C_2H_2) in the RPZ, while the NPZ is characterized by the oxidation of CO and H_2. PAH species are formed mainly in the region between RPZ and the stagnation plane. The soot formation zone is also located in this region, in which the nucleation is initiated through pyrene formation, and then the particle diameter, soot number density, and volume fraction increase continuously to their peak values. The soot oxidation mainly occurs downstream of the stagnation plane.

The presence of a double bond results in significantly higher PAH and soot emissions in 1-heptene flames compared to that in *n*-heptane flames. This is related to the increased production of C_2H_2 and C_6H_6 as a direct consequence of β scission reactions due to the presence of double bond in 1-heptene.

The PAHs and soot emissions are also strongly influenced by the level of premixing and strain rate. As the premixing level is reduced, or as ϕ is increased, the RPZ becomes weaker compared to NPZ and moves closer to the stagnation plane, while the NPZ moves away from the stagnation plane toward the oxidizer nozzle. Thus, the spatial separation between the two reaction zones decreases. However, the concentrations of C_2H_2 and PAH species increase, and consequently, the amount of soot increases, while soot oxidation decreases, with the increase in ϕ. The effect of fuel unsaturation on PAH and soot emissions becomes more pronounced as the level of premixing and/or the strain rate is reduced.

The reaction path analysis indicates two major routes for benzene formation in the RPZ. The main route is through the recombination reaction of propargyl radicals, which are mostly formed from allyl radicals. The other route is through the reaction of vinyl with butadiene. The presence of double bonds leads to the increased concentrations of propargyl and butadiene and thereby significantly more benzene in 1-heptene flames than in *n*-heptane flames. The presence of double bonds increases the amount of C_2H_2 in 1-heptene flames, since C_2H_2 is produced mainly from C_2H_4 and C_4H_5, and C_4H_5 concentration is noticeably higher in 1-heptene flames. C_2H_2 and C_6H_6 are major precursors for pyrene, while C_2H_2 also plays an important role in soot surface growth through the HACA mechanism. Thus, the presence of double bonds promotes β scission reactions leading to the increased production of C_2H_2, C_6H_6, and $C_{16}H_{10}$, and thereby higher soot emission in 1-heptene flames.

Future work will focus on performing experiments and simulations of PPFs flames with saturated and unsaturated fuel components, including long chain biodiesel surrogates such as methyl decanoate and methyl decenoate.

AUTHOR INFORMATION

Corresponding Author

*Telephone: 312-996-2235. Fax: 312-413-0441. E-mail: ska@uic.edu.

Notes

The authors declare no competing financial interest.

REFERENCES

(1) Touchard, S.; Buda, F.; Dayma, G.; Glaude, P. A.; Fournet, R.; Battin-Leclerc, F. *Int. J. Chem. Kinet.* **2005**, *37* (8), 451−463.
(2) Mehl, M.; Pitz, W. J.; Westbrook, C. K.; Yasunaga, K.; Conroy, C.; Curran, H. J. *Proc. Combust. Inst.* **2011**, *33*, 201−208.
(3) Garner, S.; Sivaramakrishnan, R.; Brezinsky, K. *Proc. Combust. Inst.* **2009**, *32*, 461−467.
(4) Minetti, R.; Roubaud, A.; Therssen, E.; Ribaucour, M.; Sochet, L. R. *Combust. Flame* **1999**, *118*, 213−220.
(5) Ribaucour, M.; Minetti, R.; Sochet, L. R. *Proc. Combust. Inst.* **1998**, *27* (1), 345−351.
(6) Vanhove, G.; Ribaucour, M.; Minetti, R. *Proc. Combust. Inst.* **2005**, *30*, 1065−1072.
(7) Prabhu, S. K.; Bhat, R. K.; Miller, D. L.; Cernansky, N. P. *Combust. Flame* **1996**, *104*, 377.
(8) Lapuerta, M.; Herreros, J. M.; Lyons, L. L.; García-Contreras, R.; Briceño, Y. *Fuel.* **2008**, *87*, 3161−3169.
(9) Schönborn, A.; Ladommatos, N.; Williams, J.; Allan, R.; Rogerson, J. *Combust. Flame* **2009**, *156*, 1396−1412.
(10) Puhan, S.; Saravanan, N.; Nagarajan, G.; Vedaraman, N. *Biomass Bioenergy* **2010**, *34*, 1079−1088.
(11) Benjumea, P.; Agudelo, J. R.; Agudelo, A. F. *Energy Fuels* **2011**, *25*, 77−85.
(12) Salamanca, M.; Mondragon, F.; Agudelo, J. R.; Benjumea, P.; Santamaría, A. *Combust. Flame* **2012**, *159*, 1100−1108.
(13) Garner, S.; Brezinsky, K. *Combust. Flame* **2011**, *158*, 2289−2301.
(14) Garner, S.; Dubois, T.; Togbe, C.; Chaumeix, N.; Dagaut, P.; Brezinsky, K. *Combust. Flame* **2011**, *158*, 2302−2313.
(15) Frenklach, M.; Wang, H. *Proc. Combust. Inst.* **1991**, *23*, 1559.
(16) Frenklach, M. *Phys. Chem. Chem. Phys.* **2002**, *4*, 2028−2037.
(17) Sarathy, S. M.; Gaïl, S.; Syed, S. A.; Thomson, M. J.; Dagaut, P. *Proc. Combust. Inst.* **2007**, *31*, 1015−1022.
(18) Fu, X.; Garner, S.; Aggarwal, S. K.; Brezinsky, K. *Energy Fuels* **2012**, *26*, 879−888.
(19) Han, X.; Aggarwal, S. K.; Brezinsky, K. *Energy Fuels* **2012**, *26*, 879−888.
(20) Domingo, P.; Vervisch, L. *Symp. Combust.* **1996**, *26*, 233−240.
(21) Berta, P. *Numerical and experimental investigation of n-heptane combustion in a counterflow configuration*. Ph.D. Thesis, University of Illinois at Chicago, Chicago, IL, 2005.
(22) Hwang, J. Y.; Chung, S. H. *Combust. Flame* **2001**, *125*, 752−62.

(23) Fisher, E. M.; Williams, B. A.; Fleming, J. W. *Proceedings of the Eastern States Section—Combustion Institute*; Combustion Institute: Pittsburgh, PA, 1997; pp 191−194.
(24) Lutz, A. E.; Kee, R. J.; Grcar, J. F.; Rupley, F. M. OPPDIF: a FORTRAN program for computing opposed flow diffusion flames. *Sandia Natl. Lab. [Tech. Rep.] SAND* **1997**, *96−8243*, UC-1404.
(25) Ranzi, E.; Dente, M.; Goldaniga, A.; Bozzano, G.; Faravelli, T. *Prog. Energy Combust. Sci.* **2001**, *27*, 99.
(26) Goldaniga, A.; Faravelli, T.; Ranzi, E. *Combust. Flame* **2000**, *122*, 350−358.
(27) Zeldovich, J. *Acta Physicochim. URSS* **1946**, *21*, 577−628.
(28) Glarborg, P.; Jensen, A. D.; Johnsson, J. E. *Prog. Energy Combust. Sci.* **2003**, *29*, 89−113.
(29) Malte, P.; Pratt, D. T. *Proc. Combust. Inst.* **1974**, *15*, 1061−1070.
(30) Guo, H.; Smallwood, G. J. *Combust. Theory Model.* **2007**, *11* (5), 741−753.
(31) Johnsson, J.; Olofsson, N.; Bladh, H.; Bengtsson, P. Laser-induced incandescence (LII). http://www.forbrf.lth.se/english/research/measurement_methods/laser_induced_incandescence_lii/ (accessed Jan. 24, 2013).
(32) Smoluchowski, M. V. *Phys Z. Chem.* **1917**, *92*, 129−139.
(33) Appel, J.; Bockhorn, H.; Frenklach, M. *Combust. Flame* **2000**, *121*, 122−136.
(34) Frenklach, M.; Harris, S. J. *J. Colloid Interface Sci.* **1987**, *118*, 252−261.
(35) Berta, P.; Aggarwal, S. K.; Puri, I. K. *Combust. Flame* **2006**, *145*, 740−764.
(36) Hwang, J. Y.; Chung, S. H. *Combust. Flame* **2001**, *125*, 752−62.
(37) Vandsburger, U.; Kennedy, I.; Glassman, I. *Combust. Sci. Technol.* **1984**, *39*, 263−85.
(38) Liu, F.; Guo, H.; Smallwood, G.; Hafi, M. *J. Quant. Spectrosc. Radiat. Transfer* **2004**, *84*, 501−511.
(39) Miller, J. A.; Melius, C. F. *Combust. Flame* **1992**, *91*, 21−39.
(40) Zhang, R. H.; Eddings, E. G.; Sarofim, A. F. *Energy Fuels* **2008**, *22* (2), 945−953.
(41) Zhang, R. H.; Eddings, E. G.; Sarofim, A. F. *Energy Fuels* **2007**, *21* (2), 677−685.